Theoretical studies of the spectroscopy of excess electrons in water clusters

R. N. Barnett and Uzi Landman
School of Physics, Georgia Institute of Technology, Atlanta, Georgia 30332

Guy Makov
School of Chemistry, The Sackler Faculty of Science, Tel Aviv University, Tel Aviv 69978, Israel

Abraham Nitzan[a)]
Department of Chemical Physics, Weizmann Institute of Science, Rehovot, 76100, Israel

(Received 11 June 1990; accepted 26 July 1990)

Variational calculation based on a continuum dielectric model, and numerical simulations based on the RWK2-M water potential and on a pseudopotential for the electron–water interaction, are used to evaluate excitation energies and optical spectra for bound interior states of an excess electron in water clusters and in bulk water. Additionally, optical data for surface states are obtained from numerical simulations. The simulation approach uses adiabatic dynamics based on the quantum-classical time-dependent self-consistent field (TDSCF) approximation and the fast-Fourier transform (FFT) algorithm for solving the Schrödinger equation. Both approaches predict very weak or no cluster size dependence of the excitation spectrum for clusters that support interior solvated electron states. For an electron attached to the cluster in a surface localization mode, bound excited states exist for most nuclear configurations of clusters down to $(H_2O)_{18}^-$, and the corresponding excitation energy is strongly shifted to the red relative to that associated with stable internal states in larger clusters. Binding and excitation energies associated with surface states are about half the value of these quantities for interior states. The present variational continuum dielectric theory is in relatively good agreement with the simulation results on the size dependence of the relative stability of interior states. However, it strongly underestimates the vertical excitation energy of the solvated electron. It is suggested that optical spectroscopy of excess electrons in water clusters could serve as a sensitive probe of the transition from surface to interior localization modes as the number of water molecules in the cluster is increased.

I. INTRODUCTION

Nonreactive electron attachment to small clusters has been a focus of many experimental[1-11] and theoretical[12-16] studies during the past few years, as part of the more general effort to elucidate the energetics and dynamics of electron solvation phenomena in molecular and ionic systems.[17-19] Recent advances in numerical simulation techniques of dynamics in mixed quantum/classical systems[14-16,19-30] and the development of reasonably reliable potentials for the water–water interaction[31-33] and pseudopotentials for the water–electrons interaction[34-36] have made it possible to study microscopic details of the localization modes, energy levels, dynamics of the solvation process, and mobility and diffusive behavior of the solvated electron. In particular, theoretical studies of these properties associated with the solvated electron in water clusters, ranging in size from two to a few hundreds water molecules, have lead to the following conclusions:

(1) The localization mode of an excess electron in water clusters depends on the cluster size. For clusters $(H_2O)_n^-$ with $n \lesssim 10$ the electron is attached in a diffuse weakly bound surface state. For $10 \lesssim n \lesssim 60$ the ground electronic state is a relatively strongly bound surface state while for $n \gtrsim 60$ the most stable state of the excess electron is a solvated state in the interior of the cluster.[35]

(2) The origin of the mode of localization (surface vs internal states) is the balance between the excess electron binding energy to the cluster and the water reorganization energy associated with the electron attachment.[35,37] For the smaller clusters the reorganization energy associated with an interior state is larger than the binding energy of this state, resulting in the preferred surface localization which requires less cluster reorganization. The opposite is true for the larger ($n \gtrsim 60$) clusters which make the interior state more stable. In intermediate size clusters ($18 \lesssim n \lesssim 60$) interior states appear as long lived metastable states. Similarly in larger clusters surface states appear as long lived metastables. [A molecular dynamics study of the time evolution from such a metastable surface state into the interior of a $(H_2O)_{256}^-$ cluster was recently carried out.[27] The surface state was found to live for more than 1 ps before penetration into the cluster's interior begins.]

(3) The electronic absorption spectrum associated with the interior solvated electron state of the larger clusters (as well as in bulk water) is weakly dependent on cluster size and is characterized by the (overlapping) transitions from the ground, *s*-like, electronic state to the three, *p*-like, lowest excited states.[26,38] The calculated absorption peak obtained from the simulation is at ~ 2.1 eV and its width of ~ 1 eV,

[a)] On leave from Tel Aviv University, Tel Aviv 69978, Israel.

 0021-9606/90/216226-13$03.00

compared to experimental results in bulk water -1.72 and 0.92 eV, respectively.[39]

(4) Vertical binding energies obtained from the simulations for the surface states of the smaller clusters ($12 \leqslant n \leqslant 18$) are in good agreement with results obtained from photoelectron spectroscopy.[40]

(5) The adiabatic dynamics of the electron solvation process (starting from the electron localized in a pre-existing trap of the neutral water), as well as the relaxation dynamics following excitation of the solvated electron, is not strongly sensitive to cluster size for clusters ($n \gtrsim 60$) that support internally bound states, and is characterized by two time scales:[19,23(a)] (a) A fast one (20–30 fs), associated with a rotational (librational) motion of the water molecules in the first solvation shell about the electron and (b) a slower relaxation stage (~ 200 fs) which is of the order of the longitudinal dielectric relaxation in water. Recent experimental results indicate however that two electronic states may be involved[41,42] with the corresponding nonadiabatic transition rate being ~ 580 fs.[42]

(6) Diffusion and mobility of the solvated electron are characterized by a nonhopping, polaron-like mechanism.[23(b),27,43] Simulations comparing "rigid" water molecules (using the RWK2 potential, with all intramolecular motion frozen at the equilibrium molecular configuration) and "flexible" water molecules (using the RWK2-M potential with all degrees of freedom free to move) show that electron migration is faster in the rigid molecules system.[43] A similar behavior was observed for the self-diffusion in water,[31,44] indicating that the flexible water system imposes stronger restrictions on the motion than the rigid water one. A related observation is that the reorganization energy is higher in the flexible water solvent than in the rigid water medium.[43]

On the experimental side, the properties of negatively charged water clusters have so far been studied using photoemission techniques.[40] From these, electron binding energies (presumably vertical) are obtained as well as information on the electron coupling to the water vibrational motion.[45,46] The recent analysis of the angular distribution of photoejected electrons from $(H_2O)_{18}^-$ has shown the potential of this method in exploring the shape and structure of such negatively charged clusters.[47] In particular, in combination with theoretical analysis, this may be a way to experimentally verify the existence of surface states predicted by the theory.

In this context we remark that based on a generalization of a dielectric continuum model of excess electron solvation to finite clusters,[37] it has been rigorously shown, and numerically simulated, that for internally localized states (described as a spherical electronic charge density in a cavity centered in a uniform dielectric sphere) the electron vertical binding energy (EVBE) varies linearly with $n^{-1/3}$, where n is the number of molecules in the cluster. It was also found from simulations[35] that the surface states for smaller clusters seem to obey such a linear relation but with a different slope. (However no rigorous justification for such behavior for the surface states is provided.) This prediction motivated analysis of recent experiments[40(a)] on hydrated electron cluster anions, $(H_2O)_n^-$ for $2 \leqslant n \leqslant 69$, where it was suggested that while indeed in small water clusters excess electrons are localized as surface states, evolving with the size of the cluster into internal states, the transition between surface to internal localization modes occurs by $n \simeq 11$, i.e., at smaller sizes than predicted by theory. At the same time it was noted that the experimental values for $n = 12$, 18, and 32 are in agreement with those predicted theoretically for the surface states of an excess electron in these clusters. We should emphasize that the above analysis of the experimental data[40(a)] is based on a straight line fit of the measured peak maxima of the photoelectron spectra, interpreted as the EVBE's, vs $n^{-1/3}$ over the *entire range* of $6 \leqslant n \leqslant 69$, whereas as noted by us before such fit is *rigorously valid only for internally localized states.*

While further analysis of photoelectron spectroscopy data and in particular for different photon energies and for larger negatively charged $(H_2O)_n^-$ clusters (i.e., $n > 69$) may help to resolve this issue, we suggest that an alternative, potentially useful way to obtain information on the states of the solvated electron is via absorption spectroscopy or resonant light scattering. This is particularly the case for cluster systems since the excited states of the attached electron provide an effective means for probing the local molecular environment and thus the excitation spectra could allow the distinction between surface versus interior localization modes. As mentioned above, our preliminary studies of the absorption spectra associated with interior states of solvated electrons in moderately large clusters ($n > 60$) indicate weak or no dependence on cluster size.[26,48] However if excited states of the surface bound electron exist, we expect that the corresponding absorption spectra will be very different from those predicted for interior states. Indeed we show in the present work that bound excited surface states exist for $(H_2O)_n^-$ clusters with $n \gtrsim 18$ and that the corresponding absorption spectrum peaks at ~ 0.85 eV, about 1.25 eV lower than the peak associated with the interior state. This difference is large enough so it may be expected that once such experiments become feasible they should be able to provide a direct unequivocal verification of the existence of excess electron surface states for clusters for which this is the stable mode of electron localization.

In addition, we present in this paper vibrational density of states spectra for neutral and negatively charged water clusters. These are obtained by Fourier transforming the nuclear velocity time correlation functions and should approximately represent the expected ir absorption spectrum of these clusters. Such "vibrational spectra" can be generated in different ways which shed light on some details of the cluster structure and the electron binding in the cluster. In particular by analyzing the spectra associated with different solvation shells about the electron we show that the solvation process is associated with a small but significant blue shift in the OH stretch frequency of the water molecules nearest to the electron. Other small shifts are observed in the intermolecular librational region of the spectrum.

Before turning to these numerical simulation studies of electronic and nuclear dynamics spectra, we consider in the next section the cluster size dependence of the electronic

energy gap between the ground and excited states of the solvated electron in a continuum dielectric model. This model, in which the cluster is represented by a sphere of dielectric function $\epsilon(\omega)$ is a generalization of continuum theories of bulk solvation. A simplified calculation using this model has shown, under certain assumptions, that once the cluster is big enough to support internal states, the electronic energy *spacing* (in contrast to the absolute positions of the electronic levels) is not sensitive to the cluster size.[48] The more rigorous treatment of Sec. II results in a weak size dependence, however this dependence is small relative to the solvent induced statistical broadening of the energy levels, seen in the simulations and reflected in the observed broad absorption. On the other hand, for surface states simple arguments predict strong red shift (relative to interior states) of both the absolute state energy and of the electronic energy gap which are seen in the simulations.

In Sec. III we present and discuss our simulation results of the electronic absorption spectra for the interior and surface states of the solvated electron. In Sec. IV we discuss different aspects of the vibrational spectra. Sec. V presents our conclusions.

II. DIELECTRIC THEORY

It has been demonstrated that continuum dielectric theory can provide reasonable estimates for the adiabatic and vertical binding energies of excess electrons in the interior states of molecular clusters, represented by dielectric spheres. In this section we use the same approach to estimate: (a) the critical cluster size that may support an internal state, and (b) the cluster size dependence of the excitation spectrum.

Consider a dielectric sphere of radius R, characterized by a static dielectric constant ϵ_s and an optical dielectric constant ϵ_∞. An electron solvated in this cluster is characterized by a wave function $\psi(\mathbf{r})$ and a charge distribution $\rho(\mathbf{r})$,

$$\rho(\mathbf{r}) = q|\psi(\mathbf{r})|^2, \tag{1}$$

where q is the electron charge.

The binding energy of the electron can be obtained as the energy associated with assembling the charge density in the dielectric medium. The latter is given by (relative to a free electron with zero momentum in vacuum)

$$W = K + \frac{1}{4\pi}\int d^3r \left(\int_0^{\mathbf{D}} \delta\mathbf{D}(\mathbf{r})\cdot\mathbf{E}(\mathbf{r}) - \int_0^{\mathbf{D}_0} \delta\mathbf{D}_0(\mathbf{r})\cdot\mathbf{E}_0(\mathbf{r}) \right), \tag{2a}$$

$$K = -\frac{\hbar^2}{2m}\int d^3r\, \psi^*(\mathbf{r})\nabla^2\psi(\mathbf{r}). \tag{2b}$$

The first term is the kinetic energy of the solvated electron (m is the electron mass) while the second is the difference between the potential energies associated with assembling the electron charge in the solvent and in vacuum.[49] In the ground state, and with the solvent at equilibrium, the displacement vector $\mathbf{D}_g$, the electric field $\mathbf{E}_g$, the polarization $\mathbf{P}_g$, and the charge distribution ρ_g, are related to each other by

$$\mathbf{P}_g = \mathbf{P}_{eg} + \mathbf{P}_{dg} = \chi_e\mathbf{E}_g + \chi_d\mathbf{E}_g = \chi_s\mathbf{E}_g, \tag{3a}$$

$$\mathbf{D}_g = \mathbf{E}_g + 4\pi\mathbf{P}_g = \epsilon_s\mathbf{E}_g, \tag{3b}$$

$$\nabla\cdot\mathbf{D}_g = 4\pi\rho_g, \tag{3c}$$

$$\chi_e = \frac{\epsilon_\infty - 1}{4\pi}, \quad \chi_d = \frac{\epsilon_s - \epsilon_\infty}{4\pi}, \quad \chi_s = \frac{\epsilon_s - 1}{4\pi}. \tag{3d}$$

χ is the dielectric susceptibility, χ_e is associated with the electronic response of the solvent (electronic polarizability of the solvent molecules) while χ_d results from the orientation of permanent solvent dipoles and from the nuclear component of the molecular polarizability. In vacuum $\chi = 0$ and $\mathbf{D}_0 = \mathbf{E}_0$. The increment $\delta\mathbf{D}$ and $\delta\mathbf{D}_0$ are associated (via the Poisson equation) with increments of the charge distribution $\delta\rho$ in the solvent and in vacuum. ϵ_s and ϵ_∞ are the static and optical dielectric constants, respectively.

The approximate nature of the following calculation should be emphasized. The use of continuum dielectric theory is an important assumption, especially for small clusters. Taking a uniform dielectric function is a further approximation in view of our knowledge, based on the numerical simulations, that the electron digs a fairly large cavity in the water due to the strong repulsion from the charge density on the oxygen atoms. Finally, for excited states, this cavity is not necessarily spherical, making the choice of excited state trial functions based on spherical symmetry (as we do below) not optimal. Nevertheless we proceed in this way in order to get a qualitative approximate description of the solvated electron and its excitations. Note that several important *relative* quantities, such as the cluster size dependence of electronic energies and energy differences between strongly bound electronic states, depend mostly on the interaction between the solvated electron and relatively distant solvent molecules. For such properties the dielectric model should be more adequate than for absolute quantities such as vertical binding energies.

We assume that the ground state is described by a $1s$ wave function and take as a convenient one parameter function

$$\psi_g(\mathbf{r}) = \left(\frac{a^3}{8\pi}\right)^{1/2} e^{-(1/2)ar}, \tag{4}$$

where a is to be determined by variation theory. For the adiabatic binding energy Eq. (2) takes the form

$$W_{gA} = K_g + \frac{1}{8\pi}\int d^3r(\mathbf{D}_g\cdot\mathbf{E}_g - |\mathbf{E}_{g0}|^2) = K_g + \frac{1}{2}\int d^3r\,\rho_g(\mathbf{r})[\phi_g(\mathbf{r}) - \phi_{g0}(\mathbf{r})], \tag{5}$$

where ϕ_g and ϕ_{g0} are the potentials associated with the charge distribution ρ_g in the presence of the dielectric sphere and in vacuum, respectively, and where $\rho_g = q|\psi_g|^2$. $\phi(\mathbf{r})$, the solution of the Poisson equation

$$\nabla^2\phi_g = \begin{cases} -4\pi\rho_g(r), & r > R \\ -\dfrac{4\pi}{\epsilon_s}\rho_g(r), & r < R \end{cases}, \tag{6}$$

can be expressed in terms of $\rho(\mathbf{r})$ in the form[50]

$$\phi(\mathbf{r}) = \int d^3r'\, \rho(\mathbf{r}')\; G(\mathbf{r},\mathbf{r}';\epsilon,R), \tag{7}$$

with the Green's function G given by

$$G(\mathbf{r},\mathbf{r}';\epsilon,R) = 4\pi \sum_{\ell=0}^{\infty} \frac{g_\ell(r,r';\epsilon,R)}{2\ell+1} \times \sum_{m=-\ell}^{\ell} Y^*_{\ell m}(\theta'\phi')\, Y_{\ell m}(\theta,\phi), \tag{8a}$$

and

$$g_\ell(r,r';\epsilon,R) = \begin{cases} \dfrac{(\epsilon-1)(\ell+1)}{\epsilon(\epsilon\ell+\ell+1)} \dfrac{r^\ell r'^\ell}{R^{2\ell+1}} + \dfrac{1}{\epsilon} \dfrac{r_<^\ell}{r_>^{\ell+1}} & (r,r'<R), \\ \dfrac{2\ell+1}{\epsilon\ell+\ell+1} \dfrac{r_<^\ell}{r_>^{\ell+1}} & \begin{pmatrix} r'<R<r \\ r<R<r' \end{pmatrix}, \\ \dfrac{r_<^\ell}{r_>^{\ell+1}} - \dfrac{\ell(\epsilon-1)}{\epsilon\ell+\ell+1} \dfrac{R^{2\ell+1}}{r^{\ell+1}r'^{\ell+1}} & (r,r'>R). \end{cases} \tag{8b}$$

For the charge distribution given by Eqs. (1) and (4), Eq. (7) can be easily evaluated. Using the results for ϕ_g and ϕ_{g0} in Eq. (5) we obtain

$$W_{gA} = \frac{\hbar^2 a^2}{8m} - \frac{5}{32} q^2 a \left(1 - \frac{1}{\epsilon_s}\right) f(aR), \tag{9a}$$

$$f(aR) \equiv 1 - \frac{16}{5}\frac{1}{aR} + \frac{16}{5}\left(1 + \frac{2}{aR}\right) e^{-aR} - \frac{4}{5}\left(\frac{1}{2}a^2R^2 + \frac{5}{2}aR + \frac{21}{4} + \frac{4}{aR}\right) e^{-2aR}. \tag{9b}$$

A minimum W_{gA} is obtained for $a_{\min}$, the solution of

$$a_{\min} = \frac{5mq^2}{8\hbar^2}\left(1 - \frac{1}{\epsilon_s}\right) g(a_{\min}R), \tag{10a}$$

$$g(aR) \equiv 1 - \frac{16}{5} e^{-aR}(1 + aR) + \frac{1}{5} e^{-2aR}(4(aR)^3 + 14(aR)^2 + 22aR + 11). \tag{10b}$$

Since $g \to 1$ for $R \to \infty$, Eq. (10a) for $a_{\min}$ can be cast in the form

$$a_{\min} = a_b g(a_{\min}R), \tag{11}$$

where the bulk limit, $a_b = a_{\min}(R \to \infty)$, is

$$a_b = \frac{5mq^2}{8\hbar^2}\left(1 - \frac{1}{\epsilon_s}\right). \tag{12}$$

Also, since $f(R \to \infty) \to 1$, Eq. (9a) leads to

$$W_{gA}(R) = W_{gA}(\infty) - \frac{5}{32} q^2 a_{\min}\left(1 - \frac{1}{\epsilon_s}\right) \times (f(a_{\min}R) - 1), \tag{13}$$

where the adiabatic binding energy in the bulk limit is

$$W_{gA}(\infty) = \frac{\hbar^2 a_b^2}{8m} - \frac{5}{32} q^2 a_b \left(1 - \frac{1}{\epsilon_s}\right). \tag{14}$$

The explicit results for bulk water ($\epsilon_s = 80$) are

$$a_b = 1.18\ \text{Å}^{-1}, \tag{15a}$$

$$\langle r^2 \rangle^{1/2} = \left(\frac{12}{a_b^2}\right)^{1/2} = 2.94\ \text{Å}, \tag{15b}$$

$$W_{gA}(\infty) = -1.32\ \text{eV}, \tag{15c}$$

and should be compared with the simulation result $\langle r^2 \rangle^{1/2} = 2$ Å, and the experimental adiabatic binding energy ~ -1.7 eV. It should be remembered that by the nature of its derivation W_{gA} is only an upper bound to the actual adiabatic binding energy of this model.

For large clusters ($a_{\min}R \to \infty$), $f(a_{\min}R)$ given in Eq. (9b) can be approximated by $f(a_{\min}R) \sim 1 - (16/5)(1/a_{\min}R)$, and using this in Eq. (13) yields

$$W_{gA}(R) = W_{gA}(\infty) + \frac{q^2}{2R}\left(1 - \frac{1}{\epsilon_s}\right) \tag{16}$$

which is identical to the result obtained previously by Barnett *et al.*[48]

Figures 1(a) and 1(b) show, as a function of the sphere size, this upper bound to the ground state energy (in units of its bulk value $= -1.32$ eV) and the "localization parameter" $a_{\min}$ (in units of $a_b = 1.18\ \text{Å}^{-1}$), respectively. There is no real solution for $a_{\min}$ for $R \leqslant R_1 \simeq 4.5$ Å. Furthermore, for $R \leqslant R_2 = 5.1$ Å, W_{gA} becomes positive, indicating that for clusters in this size range the interior s-like state is unstable or metastable relative to the ground state of a free electron. [A second solution to Eq. (11) is marked by the dotted line in Fig. 1. This is an unphysical solution for which $a \to \infty$ in the bulk limit.] Translated into number of water molecules using $R = 3a_0 n^{1/3}$ (a_0 is the Bohr radius) yields $n_1 = 22$ and $n_2 = 33$, corresponding to R_1 and R_2, respectively. Note that these numbers are related to an interior $1s$-like state, and do not reflect on the stability of a possible surface state.

The limiting result given in Eq. (16) was obtained in Ref. 48 under the assumptions that (a) the electron charge distribution is spherical, and (b) that $\rho_g(r) = 0$ for $r > R$. Figure 2 shows that indeed for spherical clusters with $R \gtrsim 5$ Å more than 90% of the electron charge in the ground $1s$ state is indeed localized within the cluster.

Consider now an abrupt change in the electron charge distribution ($\rho_g(\mathbf{r}) \to \rho_x(\mathbf{r})$), following, e.g., an optical excitation. Following this transition the electronic polarization equilibrates quickly with the new charge distribution while the nuclear polarization remains in its ground state value.[51,52] In the resulting nonequilibrium state we thus have

$$\mathbf{P}_x = \mathbf{P}_{ex} + \mathbf{P}_{dx}, \tag{17a}$$

$$\mathbf{P}_{ex} = \chi_e \mathbf{E}_x, \tag{17b}$$

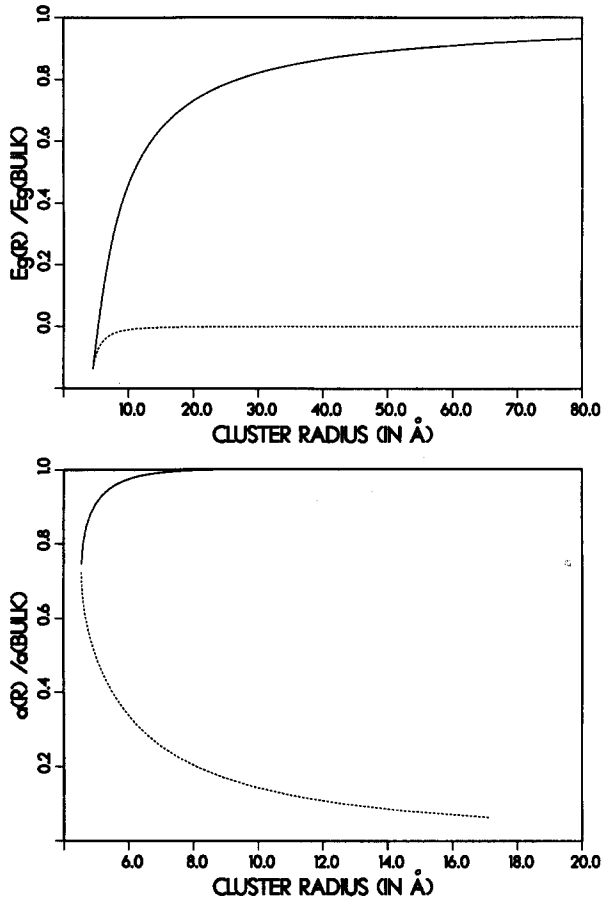

FIG. 1. (a) The upper bound to the excess electron ground state energy (in units of the bulk value $[E_g(BULK) = -1.32$ eV], versus cluster size [see Eq. (16)]. (b) The optimal value of the "localization parameter" $a_{\min}$ [see Eqs. (11) and (12)] in units of the bulk value $[a(BULK) = 1.18$ Å^{-1}] versus cluster size. The physical solution is denoted by the solid line. Dotted line corresponds to an unphysical solution for which $a_{\min} \to \infty$ in the bulk limit. The radius of the cluster (R) is given in Å.

$$\mathbf{P}_{dx} = \chi_d \mathbf{E}_g, \tag{17c}$$

$$\mathbf{D}_x = \mathbf{E}_x + 4\pi\mathbf{P}_x = (1 + 4\pi\chi_e)\mathbf{E}_x + 4\pi\chi_d\mathbf{E}_g = \epsilon_\infty \mathbf{E}_x + (\epsilon_s - \epsilon_\infty)\mathbf{E}_g, \tag{17d}$$

$$\nabla\cdot\mathbf{D}_x = 4\pi\rho_x, \tag{17e}$$

where the subscripts g and x denote the ground and excited state, respectively.

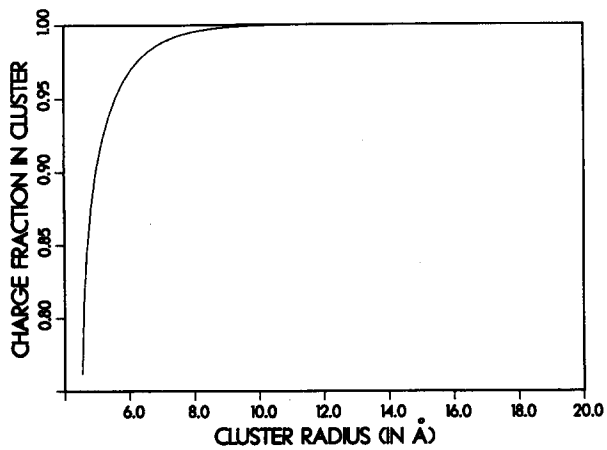

FIG. 2. Fraction of the electron charge bound in a 1s ground state versus cluster radius (in Å).

The energy difference between the initial equilibrium state g and the final nonequilibrium state x is obtained from an equation analogous to Eq. (2) (where $\int_0^D$ is replaced by $\int_{D_g}^{D_x}$). This development is outlined in Appendix A. The result is

$$\Delta E_{g\to x} = \frac{1}{2}\int d^3r(\phi_x + \phi_g)(\rho_x - \rho_g) - \frac{1}{2}\int d^3r(\rho_x\phi_{x0} - \rho_g\phi_{g0}) - \frac{\hbar^2}{2m}\int d^3r(\psi_x^*\nabla^2\psi_x - \psi_g^*\nabla^2\psi_g). \tag{18}$$

The electrostatic potentials ϕ_x and ϕ_{x0} are those associated with the charge distribution ρ_x in the presence of the sphere and in vacuum, respectively. They can be obtained from the Poisson equations

$$\nabla^2\phi_{x0} = -4\pi\rho_x(\mathbf{r}), \tag{19a}$$

and

$$\nabla^2\phi_x = \begin{cases} -4\pi\rho_x(\mathbf{r}), & r > R \\ -\dfrac{4\pi}{\epsilon_\infty}\left(\rho_x(\mathbf{r}) + \dfrac{\epsilon_\infty - \epsilon_s}{\epsilon_s}\rho_g(\mathbf{r})\right), & r < R \end{cases} \tag{19b}$$

The second of Eqs. (19b) is obtained from $\nabla^2\phi_x = -\nabla\cdot\mathbf{E}_x$ and Eqs. (17).

A particular case of Eq. (18) is that in which $\rho_x = 0$. In this case $-\Delta E_{g\to x}$ becomes the vertical binding energy of the ground state

$$W_{gV} = \frac{1}{2}\int d^3r\,\rho_g(\phi_x + \phi_g) - \frac{1}{2}\int d^3r\,\rho_g\phi_{g0} - \frac{\hbar^2}{2m}\int \psi_g^*\nabla^2\psi_g = W_{gA} + \frac{1}{2}\int d^3r\,\rho_g\phi_x, \tag{20}$$

with ϕ_x given by Eq. (19b) with $\rho_x = 0$. The solution of Eq. (19b) may be written in a form analogous to Eqs. (7) and (8)

$$\phi_x(\mathbf{r}) = \int d^3r'\,\rho_{\text{eff}}(\mathbf{r}')G(\mathbf{r},\mathbf{r}';\epsilon_s,\epsilon_\infty,R), \tag{21}$$

with

$$\rho_{\text{eff}}(\mathbf{r}) = \rho_x(\mathbf{r}) + \frac{\epsilon_\infty - \epsilon_s}{\epsilon_s}\rho_g(\mathbf{r}), \tag{22}$$

$$G(\mathbf{r},\mathbf{r}';\epsilon_s,\epsilon_\infty,R) = 4\pi\sum_{\ell=0}^{\infty}\frac{g_\ell(r,r';\epsilon_s,\epsilon_\infty,R)}{2\ell+1}\times\sum_{m=-\ell}^{\ell}Y_{\ell m}^*(\theta',\phi')Y_{\ell m}(\theta,\phi). \tag{23}$$

Evaluation of g_ℓ in Eq. (23) is performed in the same way used in Ref. 50 to evaluate g_ℓ of Eq. (8a). This evaluation is outlined, and explicit results for g_ℓ are given, in Appendix B.

In order to evaluate properties of the excited state of the solvated electron we assume, following previous molecular dynamics simulation results, that the excited state is repre-

sented by a wave function of a $2p$ symmetry and choose as a one parameter variational function the form

$$\psi_x(\mathbf{r}) = \left[\frac{b^5}{32\pi}\right]^{1/2} r e^{-br/2}\cos\theta, \tag{24}$$

where the parameter b is to be determined. As a reference consider the adiabatic situation where the excited state, Eq. (24), is in equilibrium with the bulk solvent. Using Eq. (5), with K_x, ρ_x, ϕ_x, and ϕ_{xO} replacing the ground state (g) quantities, leads to

$$W_{xA}(R=\infty) = \frac{\hbar^2 b^2}{8m} - \frac{83}{288}\frac{q^2 b}{2}\left(1-\frac{1}{\epsilon_s}\right), \tag{25}$$

which upon variation of b (to get the lowest energy state of $2p$ symmetry) yields

$$b_{\text{bulk}} = \frac{83}{288} + \frac{4m}{\hbar^2}\frac{q^2}{2}\left(1-\frac{1}{\epsilon_s}\right) \tag{26a}$$

$$\simeq 1.08\ \text{Å}^{-1}\ (\text{for } q=1 \text{ and } \epsilon_s = 80),$$

and

$$W_{xA}(\infty) = -1.1\ \text{eV}. \tag{26b}$$

Thus, according to this dielectric theory the difference between the adiabatic binding energies for the ground and excited states is 0.2 eV [compare Eqs. (15c) and (26b)].

The corresponding electron gyration radius in the excited state is given by

$$\langle r^2\rangle^{1/2} = \left(\frac{30}{b_{\text{bulk}}^2}\right)^{1/2} = 5.07\ \text{Å}. \tag{27}$$

As in the ground state [Eq. (15b)] this result is $\sim 60\%$ larger than that obtained from the simulations, however the ratio $\langle r^2\rangle_x^{1/2}/\langle r^2\rangle_g^{1/2} \simeq 1.7$ is closer to the simulation result (~ 1.5).

Consider now the vertical excitation energy in the sphere, Eq. (18). Using $\rho_g(r)$ [Eqs. (1) and (4)], $\rho_x(r)$ [Eqs. (1) and (24)] and the potentials ϕ_g [Eqs. (7) and (8)] and ϕ_x [Eqs. (21)–(23) and Appendix B], Eq. (18) can be evaluated. The algebra is quite tedious and will not be given here. The results given below were obtained using two simplifying approximations (which are shown to be valid by the molecular dynamics simulations):

(1) For clusters that support an interior solvated electron state ψ_g and ψ_x are nearly identical to their forms in the bulk dielectric [for ψ_g this is seen from the plot of $a(R)/a_b$ vs sphere radius in Fig. 1], so the main contribution to the cluster size dependence of $\Delta E_{g\to x}$ comes from the first term of Eq. (18).

(2) For such clusters the charge distribution is essentially confined to the cluster volume. For ρ_g we strictly assume $\int_{\text{sphere}} d^3r\,\rho_g(\mathbf{r}) = q$, while for ρ_x we define $f = (1/q)\int_{\text{sphere}} d^3r\,\rho_x(\mathbf{r})$ and neglect terms of order $(1-f)^2$.

We note in passing that using these approximations for ρ_g in Eq. (20) leads to an expression for $W_{gV}(R)$ obtained in a previous study,[48]

$$W_{gV} \simeq W_{gV}(\infty) + \frac{q^2}{2R}\left(1+\frac{1}{\epsilon_\infty}-\frac{2}{\epsilon_s}\right). \tag{28}$$

For $\Delta E_{g\to x}$ this procedure with these approximations leads to the following result

$$\Delta E_{g\to x}(R) = \Delta E_{g\to x}(\infty) + \frac{q^2}{2R}\left\{\frac{\epsilon_\infty - 1}{\epsilon_\infty}\frac{4.8}{2\epsilon_\infty + 3}\frac{(\langle r^2\rangle_x)^2}{R^4} - e^{-br}\left[\left(1-\frac{\epsilon_\infty}{\epsilon_s}\right)\left(\frac{3bR}{4}+1\right)+\left(1-\frac{1}{\epsilon_s}\right)\times\left(\frac{(bR)^4}{24}+\frac{(bR)^3}{12}+\frac{(bR)^2}{4}+bR+1\right)\right]\right\}, \tag{29}$$

where

$$\langle r^2\rangle_x = \int_{\text{sphere}} d^3r\, r^2|\psi_x|^2 \simeq \frac{30}{b^2} \tag{30}$$

and

$$\Delta E_{g\to x}(\infty) = \frac{1}{2}q^2\frac{5a}{16}\left(1+\frac{1}{\epsilon_\infty}-\frac{2}{\epsilon_s}\right) + \frac{\hbar^2}{8m}(b^2-a^2) + \frac{1}{2}q^2 b\left(\frac{1}{\epsilon_\infty}-1\right)\frac{83}{288} + \frac{q^2 a}{2}\left(\frac{1}{\epsilon_s}-\frac{1}{\epsilon_\infty}\right)\times\left(1-\frac{3}{2}\frac{bq^2}{(q+b)^3}-\frac{a^2}{(a+b)^2}\right). \tag{31}$$

These expressions, upon variation of b (to get the lowest energy for a state of $2p$ symmetry) and using the ground state results, yield $\Delta E_{g\to x}(\infty) = 0.38$ eV, for b = 1.18 Å. This is much smaller than the experimental result (~ 1.7 eV) and the simulation results (2.1 eV). The origin of this discrepancy may lie either in the use of a continuum dielectric theory, or in the possibly poor variational wave function chosen for the excited state.

The dependence of $\Delta E_{g\to x}$ on R is displayed in Fig. 3. While an interesting trend is observed, the most pronounced feature seen in this figure is the very weak sensitivity to cluster size for all sizes that support an interior state of the solvated electron. In a previous study[48] it was concluded that the bound–bound absorption peak associated with such interior states will not depend on cluster size. This result was derived under the assumption that the charge densities of the bound states are spherical and are well contained within the cluster. We see that our more rigorous treatment gives only a small correction to that conclusion. This is particularly so in view of the large statistical broadening observed in the com-

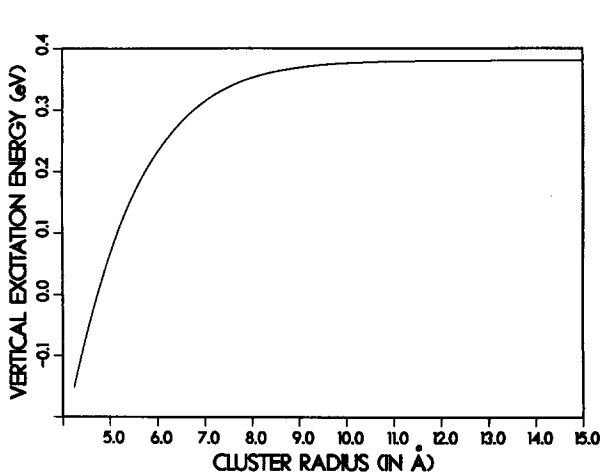

FIG. 3. Variation of the vertical excitation energy (in eV) from the ground state versus cluster radius (in Å). See Eqs. (29)–(31).

puter simulated spectra (see below) and associated with the different cluster configurations.

Finally consider the surface states. Dielectric theories of surface states[53–55] usually assume that the binding of the excess electron to the surface does not distort the (assumed spherical) shape of the cluster, resulting in a spherically symmetric wave function. However such assumptions are not valid for easily distortable molecular clusters (in fact cluster isomerization upon electron attachment has been observed also for small ionic clusters).[56] Indeed simulations show that the surface states are localized within what might be called surface cavities. This destruction of spherical symmetry makes analysis by dielectric theory complicated. A rule of thumb concerning surface state energetics is based on the observation that in an interior state the electron is in contact with twice as much dielectric medium as in the surface state and therefore the magnitude of all surface energies including the vertical excitation energy are roughly one half their bulk value. Obviously if this statement was exact, there would have been no transition from surface to bulk states as the cluster size increases, in contrast to results of numerical simulations. Still, as a rough approximation these estimates are sometimes useful.

Next we present numerical simulation results of the ground and excited states and for the absorption line shape associated with the solvated electron in water clusters and in bulk water (periodic boundary conditions).

III. MOLECULAR DYNAMICS SIMULATIONS OF ELECTRONIC SPECTRA

Method. The technical aspects of our hydrated electron simulations have been described before,[15,16,25–27] therefore we give here only a brief outline. The simulation is based on the ground state dynamics (GSD) version of the quantum-classical TDSCF approximation where the nuclei move according to the classical Newtonian equations of motion under the influence of their mutual forces and of the expectation value (with the ground electronic state, sometimes called the Hellmann–Feynman force) of the force associated with the nuclei–electron pseudopotentials. The excess electron is restricted to be in the ground state by propagating its wave function in imaginary time (using the split operator FFT algorithm) after each nuclear time step. At specific intervals along the nuclear trajectory obtained in this way, the nuclear configuration is stored and for these stored configurations higher electronic states and energies (by imaginary time propagation in conjunction with projection of lower states) are calculated. Optical absorption spectra are synthesized by constructing histograms for the frequency of occurrence of energy differences between the ground and excited electronic states, weighted by the absolute square of the transition dipoles between these states.

The potentials used in these simulations are the RKW2 (rigid molecule) and RKW2-M (flexible molecules) potential[32,33] for the intra- and intermolecular water interactions, and the pseudopotential developed by Barnett, Landman, and Jortner for the electron–water interaction.[34,35] For cluster simulations these interactions are used as they are. For bulk (periodic boundary conditions) the interactions are cut smoothly between the distances 17.5 and 18.5 a.u. The spectra reported below are based on single trajectories, 2–6 ps long, at 300 K (temperature is maintained using the stochastic collision method[57]). The classical time evolution is obtained using the velocity form of the Verlet algorithm (with an integration timestep 1.0365 fs for rigid water and 0.259 fs for flexible water). The imaginary time evolution of the electronic wave function was carried on a grid of 16^3 points for interior ground states and 32^3 points for surface states and interior excited states. The grid spacing was $1.5a_0$. Care was taken to center the wave function in the grid for both interior and surface states.

Every 8 fs the instantaneous water configuration was used to generate the three lowest excited states (contribution of higher states to the oscillator strength of transitions from the ground state was found to be small). For the interior states these correspond to three $2p$ states whose degeneracy is removed by the water molecules' distribution. Typically 300–600 such configurations (200–300 for metastable states) were used to generate each of the spectra shown below.

Energy level statistics. Figure 4 shows the energy distributions ($N(E)$) of the ground and three lowest excited states for an excess electron localized in the interior of $n = 64$, 128, and 256 water molecule clusters as well as for electrons in a system containing 256 water molecules with periodic boundary conditions (pbc) and with volume adjusted to have a mass density of 1 g/cm^3. Also shown in Fig. 4 are similar distributions for the surface states of $n = 18$, 32, and 64 water molecule clusters[58] (for $n = 64$ the result for the metastable state is marked $64s^*$). When normalized to

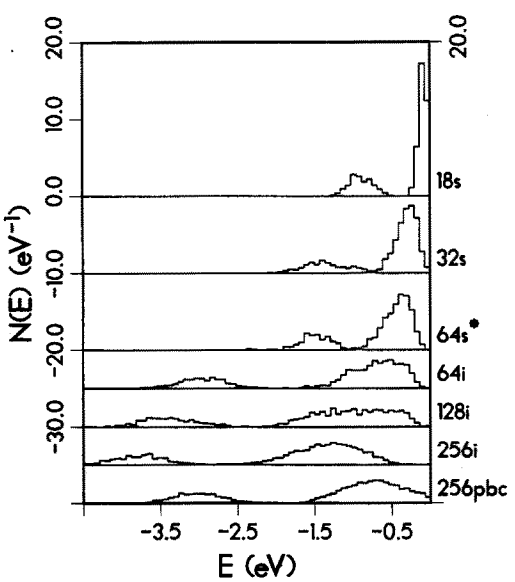

FIG. 4. Energy distributions $N(E)$ versus energy for the ground and three lowest excited states of an excess electron in water clusters, $(H_2O)_n^-$, at 300 K. For $n = 18$ and 32 the stable localization mode is in a surface state while for $n \gtrsim 64$ the electron is localized internally. For $n = 64$ $N(E)$ for both a metastable surface state (marked $64s^*$) and the stable internal state (marked $64i$) are shown. The result for bulk water (256 water molecules with periodic boundary conditions) is shown at the bottom (see text).

unity these plots represent the probabilities to observe the molecular ground and excited states with the given energies when the water is in equilibrium with the ground state of the solvated electron. For the ground state these distributions give the predicted distributions of vertical binding energies (see however below).

It is seen that both for interior and for surface states the energies of the ground and excited states shift to lower energies (larger magnitude) upon increasing the cluster size. In general, the energies for the surface states are about one half of the interior states values, as discussed above. The widths of these distributions (~ 1 eV for internal states, ~ 0.5 eV for surface states) arise from the dependence of the solvated electron energy levels on the instantaneous equilibrium water molecule configurations in the cluster. It should be kept in mind that the excited state distributions represent overlapping peaks of the three lower excited states.

While our accumulated experience in studying these spectra leads us to strongly believe that all energy differences (widths, relative peak positions, line shift associated with cluster size, etc.) are correctly represented (within the model) by these results, a measure of caution is required with regard to the absolute energies. Consider, e.g., the average ground state vertical binding energy. For bulk water simulations Rossky and co-workers[36,38] report this energy to be ~ 3 eV (using SPC intermolecular interaction, i.e., rigid molecules, the electron–water pseudopotential from Ref. 36, and 500 water molecules with periodic boundary conditions), in good agreement with current experimental estimates. We get a similar result in our bulk water simulations (256 molecules with pbc's and potential cutoff at ~ 18 a.u.).[59] However it is seen from Fig. 4 that the shift to lower energies does not saturate at system sizes of a few hundred molecules. In fact dielectric continuum theory predicts that the electron cluster interaction will behave like $(1/R)$ for large R and cluster simulation results confirm this expectation. For bulk simulations this $(1/R)$ behavior can hold only up to the cutoff applied to the electron water interaction and, in any case, for distances no longer than half of the linear dimension of the system's periodically replicated calculational cell. In fact, using pbc's disturbs the $1/R$ behavior also for smaller distances because under such conditions the solvent polarization vanishes at the boundary, implying that it is artificially reduced also close to the boundary, inside the system.

This is the main reason for the difference seen in Fig. 4 between the energy band positions of the $(H_2O)_{256}^-$ cluster and the electron solvated in a "bulk" composed of 256 water molecules with pbc's. A smaller contribution to this difference arises from the difference in molecular density in the interior of the cluster (~ 1.07 g/cm^3) and in the "Bulk" (1 g/cm^3).

One implication of the above discussion is that the problem of the actual magnitude of the EVBE [the electronic (ground state) vertical binding energy] is not yet settled (as we expect the results of Ref. 36 and 38 to be affected in the same way as discussed above). Extrapolating the results obtained from finite clusters to $R \to \infty$, using a fit to $1/R$ for large R results in EVBE$\simeq -5.1$ eV, considerably lower (larger magnitude) than current experimental estimates based on photoelectron spectroscopy.[40] This issue deserves further study both on the experimental and the theoretical side.

From the point of view of the present work, the important fact is that energy *differences* are not affected by the above considerations. The reason for this is that the issue discussed above is mainly associated with the solvent polarization far from the electron. At such distances the magnitude of the electric field of the electron is simply q/r^2, independent of the detailed shape of the electron charge distribution. These long range effects are therefore canceled in the calculation of energy spacings (i.e., absorption spectra).

Electronic absorption spectra. Figure 5 displays the simulated (bound–bound) absorption spectra for the interior states of $(H_2O)_n^-$ clusters ($n = 64,128,256$), for an electron solvated in "bulk" water (defined above) and for surface states in $(H_2O)_n^-$ clusters ($n = 18,32,64$).[58] These results emphasize three striking features already mentioned before: (a) There exist excited bound surface states of negative water clusters with $n \geqslant 18$. (b) The absorption bands associated with surface states peak at energies considerably lower than those associated with interior states (~ 0.82 eV and ~ 2.1 eV, respectively). Within their localization categories (surface or interior state spectra) the absorption bands are largely insensitive to the cluster sizes.[60]

The very pronounced difference between the bound to bound absorption bands of surface and interior states is potentially a useful way for observing the predicted transition from surface to bulk states as a function of cluster size. (In this context we note that we have previously observed such a marked blue shift in studies of electron penetration into large clusters of water.[27]) Previous attempts to observe this tran-

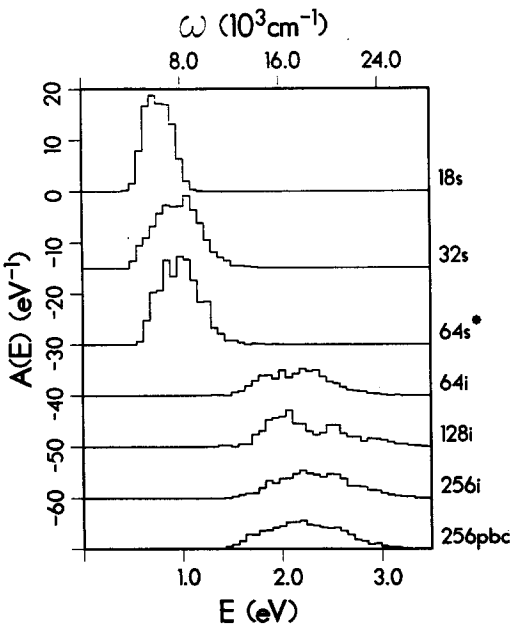

FIG. 5. Spectra $A(E)$ for surface and internal states of an excess electron in $(H_2O)_n^-$ clusters, at 300 K as well as for an electron in bulk water (see caption to Fig. 4).

sition in the edge of photoelectron spectra have not given a definite answer.

Finally, we note that as expected, the reported energy distributions and absorption bands are not sensitive to whether a rigid (RWK2) or a flexible (RWK2-M) model is used to describe the water molecules.

IV. VIBRATIONAL DENSITY OF STATES

The normalized vibrational density of states is obtained from the Fourier transform of the velocity time-correlation function according to

$$g(\omega) = (\pi\phi(0))^{-1} \int_{-\infty}^{\infty} dt\, \phi(t) e^{i\omega t}, \tag{32a}$$

where

$$\phi(t) = \sum_{i=1}^{N} m_i \mathbf{v}_i(0) \cdot \mathbf{v}_i(t), \tag{32b}$$

with m_i and $\mathbf{v}_i$ being the mass and velocity of atom i and $\phi(0) = n_d k_B T$, where n_d is the number of degrees of freedom ($n_d = 3N$ if no constraints are imposed on the motion). We can focus on the separate contributions, $g_O(\omega)$ and $g_H(\omega)$, of the oxygen and hydrogen atoms to the density of states by limiting the sum in Eq. (32b) to atoms of the particular species [thus $g(\omega) = 1/3(2g_H(\omega) + g_O(\omega)]$. Furthermore the contribution to the density of states associated with a particular group of water molecules (e.g., a particular solvation shell about the electron) can be obtained by limiting the sum in Eq. (32b) to atoms in this group only.

The spectra shown in Figs. 6 and 7 are based on 15 ps trajectories in systems of 256 water molecules. Figure 6 shows the vibrational densities of states associated with water molecules in 3 different water solvation layers about the solvated electron. Within the statistical errors of this calculation the spectrum associated with molecules further than 10 a.u. from the electron center, but not including those in the outer periphery of the cluster, is the same as that obtained in neutral bulk water. Therefore the difference between the spectrum obtained from the inner shell (dashed line) and between that associated with the outer shell (full line) reflect the effect of the solvated electron on the vibrational motion of neighboring water molecules. Three main effects are seen.

(a) For the water molecules nearest to the electron, intensity in the stretch spectral region (~ 3700 cm^{-1}) shifts to the blue and a sharp peak is seen ~ 200 cm^{-1} higher than the bulk peak [see Fig. 6(b)]. The position of the sharp peak is characteristic of the O–H stretch vibration in the *free* water molecule and the 200 cm^{-1} red shift seen in bulk water is due to the formation of the H-bonded network. This network is partially destroyed in the first solvation shell about the electron and as a result the intramolecular motion acquires a free molecule character.

(b) In the region of the spectrum associated with librational motion ($200 \lesssim \omega \lesssim 1000$ cm^{-1}) intensity is shifted to the red. This is seen more strongly in the partial spectrum associated with the hydrogen atoms [Fig. 6(b)] which are the main origin of this part of the spectrum.

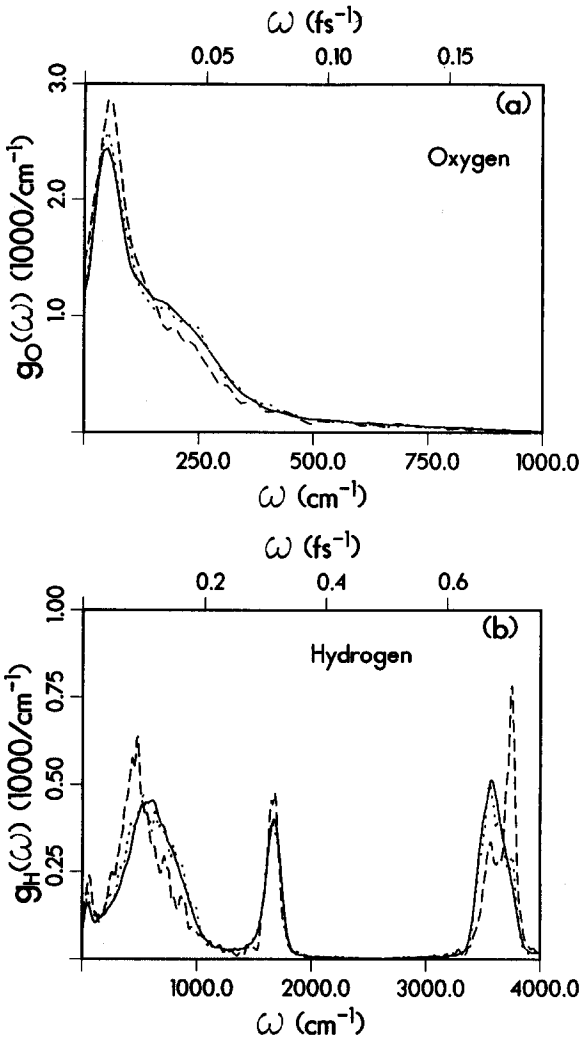

FIG. 6. Vibrational densities of state for the oxygens [$g_O(\omega)$, in (a)] and hydrogens [$g_H(\omega)$, in (b)] of water in the presence of a solvated electron in a $(H_2O)_{256}^-$ cluster, at 300 K. The vibration spectra for molecules in the first and second solvation shells about the excess electron are denoted by dashed and dotted lines, respectively, and those for water molecules beyond the second solvation shell (but not including those at the periphery of the cluster) are denoted by a solid line. $g(\omega)$ in units of 10^3/cm^{-1} and ω in units of cm^{-1} (bottom axis) and fs^{-1} (top axis).

(c) In the spectral region associated with translational motion ($\omega \lesssim 100$ cm^{-1}) intensity is shifted to the blue. This is seen more clearly in Fig. 6(a) which displays the partial spectrum associated with the oxygen atoms.

In Fig. 7 we compare the intermolecular part of the vibrational spectrum for neutral "bulk" water using rigid water molecules (dashed line) and flexible water molecules (full line). It is interesting to note that the two spectra are similar indicating weak coupling between the intramolecular and intermolecular motions in water. This observation justifies the use of rigid water models for simulation of ion and electron solvation phenomena, however we note that in recent work we[43] as well as others[44] have found that the two models give different transport coefficients both for the self-diffusion of water[44] and for the mobility of the solvated electron.[43]

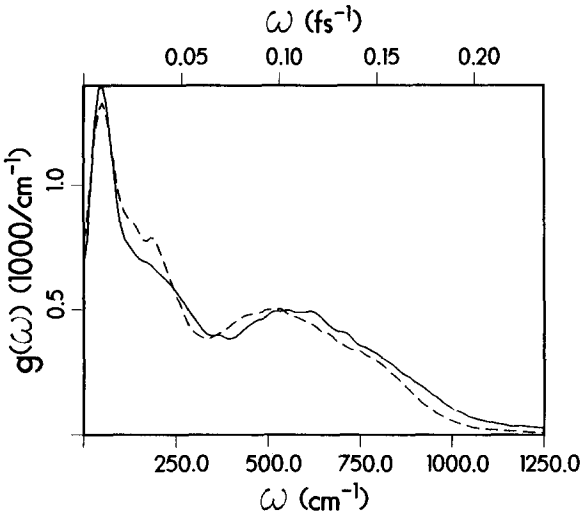

FIG. 7. The intermolecular part of the vibrational spectrum for neutral bulk water at 300 K, simulated by using rigid water molecules (dashed line) or flexible ones (solid line). Since both spectra are normalized to unity and the flexible system has 1.5 more modes than the rigid one, the spectrum for the flexible system was multiplied by 1.5 to make the comparison easier. $g(\omega)$ in units of $10^3/\mathrm{cm}^{-1}$ and ω in units of cm^{-1} (bottom axis) and fs^{-1} (top axis).

V. CONCLUSIONS

In this paper we have applied both continuum dielectric theory and comparatively sophisticated simulation methods based on state of the art interaction potentials to study the cluster size dependence of excited states and excitation spectra of an excess electron in water clusters. The continuum dielectric theory was limited to interior electron states in dielectric spheres, while numerical simulations where used to study both interior states (in large enough clusters) and surface states.

The main results of our numerical simulations are

(a) Surface states of an excess electron in water clusters, $(H_2O)_n^-$ ($n \geqslant 18$) support up to three excited states. [For large clusters ($n \geqslant 64$) the surface localization mode is metastable.]

(b) The stable interior ground electron states in clusters of size $64 \lesssim n \leqslant 256$ correspond to cluster configurations which support at least three excited (p-like) states.

(c) Excitation spectra associated with the ground interior (surface) states show very weak or no dependence on the cluster size. However large differences exist between surface and interior state spectra. Surface state energies (and positions of spectral peaks) are roughly half the size of the interior state values.

The results of continuum dielectric theory show many qualitative similarities to those of the numerical simulations, and in particular the loss of stability of interior states (relative to the neutral cluster) is predicted by this theory to be at about $n = 30$–40, similar to the simulation result. However the dielectric theory supplemented by a quantum mechanical variational calculation of the electron states strongly underestimate the vertical transition energy from the s-like ground electron state to the p-like lowest excited state. This calculation also predicts a very weak cluster size dependence of this excitation energy (a small blue shift when n increases from $n \sim 60$ to the bulk limit). This effect is smaller than the statistical uncertainty of our simulation results, and is probably also too small to be observed experimentally. On the other hand the difference between the spectra of surface states and of interior states is very pronounced and may potentially be a way to distinguish unambiguously between these types of electron binding to water clusters.

ACKNOWLEDGMENTS

This research was supported by the U. S. Department of Energy Grant No. FG05-86ER45234, by the Israel Academy of Science, and by the Israel–USA BSF.

APPENDIX A: VERTICAL EXCITATION ENERGIES

Consider a transition from a fully equilibrated ground state to an excited state, where only the electronic polarization is in equilibrium with the excited state, while the nuclear polarization remains in its ground state value.

The energy of the electron in the excited state may be obtained from an equation analogous to Eq. (2) (relative to a free electron with zero momentum),

$$W_x = K_x + \frac{1}{4\pi}\int d^3r \times\left[\int_0^{\mathbf{D}_x} \delta\mathbf{D}(\mathbf{r})\cdot\mathbf{E}(\mathbf{r}) - \int_0^{\mathbf{D}_{x0}} \delta\mathbf{D}_0(\mathbf{r})\cdot\mathbf{E}_0(\mathbf{r})\right], \quad \text{(A1a)}$$

$$K_x = -\frac{\hbar^2}{2m}\int d^3r\, \psi_x^*(\mathbf{r})\nabla^2\psi_x(\mathbf{r}), \quad \text{(A1b)}$$

where $\mathbf{E}_0 = \mathbf{D}_0$ is the field for $\epsilon = 1$.

The integral in Eq. (A1a) may be evaluated by considering the change in $\mathbf{D}$ to occur in two steps.[51] First $\mathbf{D}(\mathbf{r})$ changes from zero throughout the dielectric to $\mathbf{D}_g(\mathbf{r})$, which is its value in the fully equilibrated ground state. Then it changes from $\mathbf{D}_g(\mathbf{r})$ to $D_x(\mathbf{r})$, which is its value in the vertically excited state, under the constraint that the nuclear polarization $\mathbf{P}_d(\mathbf{r})$ remains unchanged and equal to its ground state value $\mathbf{P}_{dg}(\mathbf{r})$.

We may now write the energy of the excited state as

$$W_x = K_x + \frac{1}{4\pi}\int d^3r \left[\int_0^{\mathbf{D}_x} \delta\mathbf{D}(\mathbf{r})\cdot\mathbf{E}(\mathbf{r}) + \int_{\mathbf{D}_g}^{'\mathbf{D}_x} \delta\mathbf{D}(\mathbf{r})\cdot\mathbf{E}(\mathbf{r}) - \int_0^{\mathbf{D}_{g0}} \delta\mathbf{D}_0(\mathbf{r})\cdot\mathbf{E}_0(\mathbf{r}) - \int_{\mathbf{D}_{g0}}^{\mathbf{D}_{x0}} \delta\mathbf{D}_0(\mathbf{r})\cdot\mathbf{E}_0(\mathbf{r})\right], \quad \text{(A2)}$$

where the prime in the second integral denotes integration along a path with the constraint $P_d = P_{dg}$.

The vertical excitation energy $\Delta E_{g\to x}$ is the difference between the energy of the electron excited from the ground state [given by (A2)] and the binding energy of the electron in the ground state [given by Eq. (2)] and is equal to

$$\Delta E_{g\to x} = K_x - K_g + \frac{1}{4\pi}\int d^3r\left[\int_{D_g}^{D_x}\delta\mathbf{D}(\mathbf{r})\cdot\mathbf{E}(\mathbf{r}) - \int_{D_{g0}}^{D_{x0}}\delta\mathbf{D}_0(\mathbf{r})\cdot\mathbf{E}_0(\mathbf{r})\right]. \quad \text{(A3)}$$

From Eq. 17(d) we can see that the constraint $\mathbf{P}_d = \mathbf{P}_{dg}$ throughout the transition means that

$$\delta\mathbf{D} = \epsilon_\infty\,\delta\mathbf{E}, \quad \text{(A4)}$$

instead of $\delta\mathbf{D} = \epsilon_s\delta\mathbf{E}$.

The integral over $\delta\mathbf{D}$ may now be performed to yield

$$I = \frac{1}{4\pi}\int d^3r\int_{D_g}^{D_x}\delta\mathbf{D}\cdot\mathbf{E} = \frac{\epsilon_\infty}{8\pi}\int d^3r\left[\mathbf{E}_x^2(r) - \mathbf{E}_g^2(r)\right]. \quad \text{(A5)}$$

Using the definitions

$$\mathbf{E}_x = -\nabla\phi_x, \quad \mathbf{E}_g = -\nabla\phi_g, \quad \text{(A6)}$$

this integral may be rewritten

$$I = \frac{\epsilon_\infty}{8\pi}\int d^3r(\nabla\phi_x + \nabla\phi_g)(\nabla\phi_x - \nabla\phi_g) = \frac{\epsilon_\infty}{8\pi}\int d^3r(\phi_x + \phi_g)(\nabla^2\phi_g - \nabla^2\phi_x), \quad \text{(A7)}$$

where the last transformation involves applying Green's first theorem. Using Eqs. (6), (17d), and (17e) we find that

$$\nabla^2\phi_x = -\frac{4\pi\rho_x(\mathbf{r})}{\epsilon_\infty} + \left(\frac{1}{\epsilon_\infty} - \frac{1}{\epsilon_s}\right)4\pi\rho_g(\mathbf{r}), \quad \text{(A8)}$$

which may be inserted into the integral to find

$$I = \frac{1}{2}\int d^3r(\phi_x + \phi_g)(\rho_x - \rho_g). \quad \text{(A9)}$$

Thus the vertical excitation energy given by Eq. (A3) is given explicitly as

$$\Delta E_{g\to x} = \frac{1}{2}\int d^3r(\phi_x + \phi_g)(\rho_x - \rho_g) - \frac{1}{2}\int d^3r(\rho_x\phi_{x0} - \rho_g\phi_{g0}) - \frac{\hbar^2}{2m}\int d^3r(\psi_x^*\nabla^2\psi_x - \psi_g^*\nabla^2\psi_g). \quad \text{(A10)}$$

APPENDIX B: SOLUTION OF A POISSON TYPE EQUATION IN THE NONEQUILIBRIUM CASE

The electric potential ϕ_x immediately after an optical transition is the solution of a Poisson type equation [Eq. (19b)],

$$\nabla^2\phi_x = -\frac{4\pi\rho_x(\mathbf{r})}{\epsilon_\infty} + \left(\frac{1}{\epsilon_\infty} - \frac{1}{\epsilon_s}\right)4\pi\rho_g(\mathbf{r}). \quad \text{(B1)}$$

By rearranging the terms in (B1)

$$\nabla^2\phi_x = -\frac{4\pi}{\epsilon_\infty}\rho_{\text{eff}}(\mathbf{r}), \quad \text{(B2a)}$$

$$\rho_{\text{eff}}(\mathbf{r}) \equiv \rho_x(\mathbf{r}) + \frac{(\epsilon_\infty - \epsilon_s)}{\epsilon_s}\rho_g(\mathbf{r}). \quad \text{(B2b)}$$

This now has the usual form of a Poisson equation and may be solved (as described in Ref. 50), subject to the boundary conditions as detailed below.

As in the equilibrium case [Eqs. (6)–(8)] the solution is given by

$$\phi_x(\mathbf{r}) = \int d^3r'\rho_{\text{eff}}(\mathbf{r}')G^x(\mathbf{r},\mathbf{r}';\epsilon_s,\epsilon_\infty,R). \quad \text{(B3)}$$

The Green's Function G^x may be expanded in spherical harmonics

$$G^x(r,r';\epsilon_s,\epsilon_\infty,R) = 4\pi\sum_{\ell=0}^{\infty}\frac{g_\ell^x(r,r';\epsilon_s,\epsilon_\infty,R)}{2\ell+1}\times\sum_{m=-\ell}^{\ell}Y_{\ell m}^*(\theta',\phi')Y_{\ell m}(\theta,\phi). \quad \text{(B4)}$$

The functions $g_\ell^x(r,r';\epsilon_s,\epsilon_\infty,R)$ may be found explicitly by solving for a point charge q at r'.

Following Bottcher[50] we seek a solution for ϕ_x of the form

$$\phi_x(\mathbf{r}) = \begin{cases} 4\pi\sum_{\ell=0}^{\infty}\left(A_\ell r^\ell + \frac{B_\ell}{r^{\ell+1}}\right)\frac{Y_{\ell m}^*(\theta',\phi')Y_{\ell m}(\theta,\phi)}{2\ell+1} & (r>R) \\ 4\pi\sum_{\ell=0}^{\infty}\left(C_\ell r^\ell + \frac{D_\ell}{r^{\ell+1}}\right)\frac{Y_{\ell m}^*(\theta',\phi')Y_{\ell m}(\theta,\phi)}{2\ell+1} & (r<R) \end{cases} \quad \text{(B5)}$$

Denoting the solution for $r>R$ as ϕ_1 and for $r<R$ as ϕ_2, the boundary conditions (BC) are

BC I: $\phi_1(r=R) = \phi_2(r=R)$, (B6a)

BC II: $\phi_1(r\to\infty) = 0$, (B6b)

BC III: $\left.\frac{\partial\phi_1}{\partial r}\right|_{r=R} = \epsilon_\infty\left.\frac{\partial\phi_2}{\partial r}\right|_{r=R} - 4\pi\mathbf{P}_d\big|_{r=R}$, (B6c)

$$\mathbf{P}_d = \frac{\epsilon_s - \epsilon_\infty}{4\pi}\mathbf{E}_g = -\frac{\epsilon_s - \epsilon_\infty}{4\pi}\frac{\partial\phi_g}{\partial r}, \quad \text{(B6d)}$$

where ϕ_g is the electric potential in the ground state at equilibrium.

The rhs of the third BC [Eq. (B6)] is derived from the requirement that the perpendicular element of the electric displacement be continuous at the interface. Inside the di-

electric sphere the electric displacement is given by Eq. (17d) as

$$\begin{aligned}\mathbf{D}_x &= (1+4\pi\alpha_e)\mathbf{E}_x + 4\pi\alpha_d\mathbf{E}_g \\ &= \epsilon_\infty \mathbf{E}_x + 4\pi\alpha_d\mathbf{E}_g \\ &= -\epsilon_\infty \nabla\phi_x - (\epsilon_s-\epsilon_\infty)\nabla\phi_g, \qquad \text{(B7)}\end{aligned}$$

$$\mathbf{D}_x = -\epsilon_\infty \left.\frac{\partial\phi_x}{\partial r}\right|_{r=R} - (\epsilon_s-\epsilon_\infty)\left.\frac{\partial\phi_g}{\partial r}\right|_{r=R}. \qquad \text{(B8)}$$

Following the discussion in Bottcher[50] we find for the case $r'<r<R$

$$D_\ell = \frac{qr'^\ell}{\epsilon_\infty}, \qquad \text{(B9)}$$

and from Eq. (B6b) we find $A_\ell = 0$. Using Eq. (B6a),

$$\frac{B_\ell}{R^{\ell+1}} = C_\ell R^\ell + \frac{qr'^\ell}{\epsilon_\infty} \qquad \text{(B10)}$$

and finally, from Eq. (B6),

$$\begin{aligned}\frac{-(\ell+1)B_\ell}{R^{\ell+2}} &= \epsilon_\infty\left[\ell C_\ell R^{\ell-1} - \frac{(\ell+1)qr'^\ell}{\epsilon_\infty R^{\ell+2}}\right] \\ &\quad + 4\pi(\epsilon_s-\epsilon_\infty)\left.\frac{\partial\phi_g}{\partial r}\right|_{r=R}\delta_{\ell,0}. \qquad \text{(B11)}\end{aligned}$$

Equations (B10) and (B11) may now be solved to find the coefficients B_ℓ and C_ℓ. The results are

$$B_\ell = \frac{(2\ell+1)}{\epsilon_\infty\ell+\ell+1}qr'^\ell - \delta_{\ell,0}(\epsilon_s-\epsilon_\infty)4\pi R^2\left.\frac{\partial\phi_g}{\partial r}\right|_{r=R}, \qquad \text{(B12a)}$$

$$C_\ell = \frac{(\epsilon_\infty-1)(\ell+1)}{\epsilon_\infty(\epsilon_\infty\ell+\ell+1)}\frac{qr'^\ell}{R^{2\ell+1}} - \delta_{\ell,0}(\epsilon_s-\epsilon_\infty)4\pi R^2\left.\frac{\partial\phi_g}{\partial r}\right|_{r=R}. \qquad \text{(B12b)}$$

These results may be generalized for the case $r<r'<R$ by replacing r' by $r_<$ and r by $r_>$ in Eqs. (B5), (B8), and (B12). $r_<$ refers to the smaller of (r,r') and $r_>$ to the larger of the pair.

Next, consider the case where $r'>R$, i.e., the charge q is outside the dielectric sphere. The boundary conditions I and III remains unchanged, while Eq. (B6b) is replaced by the requirement that ϕ is well behaved throughout the sphere and in particular at $r=0$. This requirement yields

$$D_\ell = 0. \qquad \text{(B13)}$$

In an analogous manner to the previous case of $r'<R$ we find

$$A_\ell = \frac{q}{r'^{\ell+1}}, \qquad \text{(B14a)}$$

$$B_\ell = -\frac{\ell(\epsilon_\infty-1)}{(\epsilon_\infty\ell+\ell+1)}\frac{qR^{2\ell+1}}{r'^{\ell+1}} - \delta_{\ell,0}(\epsilon_s-\epsilon_\infty)4\pi R^2\left.\frac{\partial\phi_g}{\partial r}\right|_{r=R}, \qquad \text{(B14b)}$$

$$C_\ell = -\frac{(2l+1)}{\epsilon_\infty\ell+\ell+1}\frac{q}{r'^{\ell+1}} - \delta_{\ell,0}(\epsilon_s-\epsilon_\infty)4\pi R\left.\frac{\partial\phi_g}{\partial r}\right|_{r=R}. \qquad \text{(B14c)}$$

The function $g_\ell^x(r,r';\epsilon_s,\epsilon_\infty,R)$ from Eq. (B4) may now be obtained using Eqs. (B5), (B8), (B12)–(B14) yielding

$$g_\ell^x = \begin{cases} \dfrac{(\epsilon_\infty-1)(\ell+1)}{\epsilon_\infty(\epsilon_\infty\ell+l+1)}\dfrac{r^\ell r'^\ell}{R^{2\ell+1}} - \delta_{\ell,0}(\epsilon_s-\epsilon_\infty)\dfrac{4\pi R}{\rho_{eff}(r')}\left[\nabla_{r'}\left.\dfrac{\partial\phi_g(r)}{\partial r}\right|_{r=R}\right] + \dfrac{r_<^\ell}{\epsilon_\infty r_>^{\ell+1}} & (r,r'<R) \quad \text{(B15a)} \\ \dfrac{(2\ell+1)r_<^\ell}{(\epsilon_\infty\ell+l+1)r_>^{\ell+1}} - \delta_{\ell,0}(\epsilon_s-\epsilon_\infty)\dfrac{4\pi R}{r\rho_{eff}(r')}\left[\nabla_{r'}\left.\dfrac{\partial\phi_g(r)}{\partial r}\right|_{r=R}\right] & (r'<R<r) \quad \text{(B15b)} \\ \dfrac{(2\ell+1)r_<^\ell}{(\epsilon_\infty\ell+l+1)r_>^{\ell+1}} - \delta_{\ell,0}(\epsilon_s-\epsilon_\infty)\dfrac{4\pi R}{\rho_{eff}(r')}\left[\nabla_{r'}\left.\dfrac{\partial\phi_g(r)}{\partial r}\right|_{r=R}\right] & (r<R<r') \quad \text{(B15c)} \\ \dfrac{r_<^\ell}{r_>^{\ell+1}} - \dfrac{\ell(\epsilon_\infty-1)}{(\epsilon_\infty l+l+1)}\dfrac{R^{2\ell+1}}{r^{\ell+1}r'^{\ell+1}} - \dfrac{\delta_{\ell,0}(\epsilon_s-\epsilon_\infty)4\pi R^2}{r\rho_{eff}(r')}\left[\nabla_{r'}\left.\dfrac{\partial}{\partial r}\phi_g(r)\right|_{r=R}\right] & (R<r,r'), \quad \text{(B15d)} \end{cases}$$

where as before r refers to the smaller of r and r' while $r_>$ refers to the larger.

[1] M. Armbuster, H. Haberland, and H. G. Schindler, Phys. Rev. Lett. **47,** 323 (1981).

[2] H. Haberland, H. Langosch, H. G. Schindler, and D. R. Worsnop, Surface Sci. **156,** 517 (1985).

[3] H. Haberland, H. G. Schindler, and D. R. Worsnop, Ber. Bunsenges. Phys. Chem. **88,** 270 (1984).

[4] H. Haberland, H. G. Schindler, and D. R. Worsnop, J. Chem. Phys. **81,** 3742 (1984).

[5] M. Knapp, O. Echt, D. Kreisle, and E. Recknagel, J. Chem. Phys. **85,** 636 (1986); J. Phys. Chem. **91,** 2601 (1987).

[6] (a) K. H. Bowen, Z. Phys. D (in press); (b) S. T. Arnold, J. G. Eaton, D. Patel-Misra, H. W. Sarkas, and K. H. Bowen, in *Ion Cluster Spectroscopy and Structure*, edited by J. P. Maier (Elsevier, New York, 1989).

[7] See articles in *Elemental and Molecular Clusters*, edited by G. Benedek, T. P. Martin, and G. Pacchioni (Springer-Verlag, Berlin, 1988).

[8] T. M. Miller, D. G. Leopold, K. K. Murray, and W. C. Lineberger, J. Chem. Phys. **85,** 2368 (1986), and references therein.

[9] T. P. Martin, Phys. Rep. **95,** 167 (1983), and references therein.

[10] (a) M. Kappes, P. Radi, M. Schar, and E. Schumacher, Chem. Phys. Lett. **113,** 243 (1985); (b) K. I. Peterson, P. D. Dao, and A. W. Castelman, Jr., J. Chem. Phys. **79,** 777 (1983); (c) E. C. Honea, M. L. Homer, P. Labastie, and R. L. Whetten (to be published); (d) M. Kappas (to be published).

[11] (a) C. L. Pettiette, S. H. Yang, M. J. Craycraft, J. Conceicao, R. T. Laaksonen, O. Cheshnovsky, and R. E. Smalley, J. Chem. Phys. **88,** 5377 (1988); (b) D. G. Leopold and W. C. Lineberger, *ibid.* **86,** 1715 (1987).

[12] K. D. Jordan, Acc. Chem. Res. **12,** 36 (1979).

[13] J. Jortner, J. Ber. Bunsenges. Phys. Chem. **88,** 188 (1984).

[14] (a) B. J. Berne and D. Thirumalai, Annu. Rev. Phys. Chem. **37,** 401 (1986); (b) M. Sprik and M. Klein, Comp. Physics Reports **7,** 147 (1988).
[15] U. Landman, R. N. Barnett, C. L. Cleveland, J. Luo, D. Scharf, and J. Jortner, in *Few Body Systems and Multiparticle Dynamics*, edited by D. Micha (American Institute of Physics, New York, 1987), p. 200; U. Landman, in *Recent Developments in Computer Simulation Studies in Condensed Matter Physics*, edited by D. P. Landau, K. K. Mon, and H. B. Schuttler (Springer, Berlin, 1988), p. 144; J. Jortner, D. Scharf, and U. Landman, in Ref. 7, p. 148; R. N. Barnett, U. Landman, D. Scharf, and J. Jortner, Acct. Chem. Res. **22,** 350 (1989).
[16] R. N. Barnett, U. Landman, G. Rajagopal, and A. Nitzan, Israel J. Chem. **30,** 85 (1990).
[17] For reviews and collections see (a) *Physics of Ionic Solvation*, edited by Ulstrup (Elsevier, Amsterdam, 1986); (b) Farady Disc. Chem. Soc. **85,** (1988); (c) E. M. Kosower and D. Huppert, Ann. Rev. Phys. Chem. **37,** 127 (1986).
[18] *The Chemical Physics of Solvation*, edited by R. R. Dojonadze, E. Kalman, A. A. Kornyshev, and J. Ulstrup (Elsevier, Amsterdam, 1986).
[19] R. N. Barnett, U. Landman, and A. Nitzan, J. Chem. Phys. **90,** 4413 (1989), and references therein.
[20] M. Parrinello and A. Rahman, J. Chem. Phys. **82,** 860 (1985).
[21] R. Kosloff, J. Phys. Chem. **92,** 2087 (1988).
[22] D. Kumamoto and R. Silbey, J. Chem. Phys. **75,** 5164 (1981).
[23] (a) P. J. Rossky and J. Schnitker, J. Phys. Chem. **92,** 4277 (1988), and references therein; (b) P. J. Rossky and J. Schnitker, *ibid.* **93,** 6965 (1989).
[24] D. F. Coker and B. J. Berne, J. Chem. Phys. **89,** 2128 (1988).
[25] R. N. Barnett, U. Landman, and A. Nitzan, Phys. Rev. A **38,** 2178 (1988).
[26] R. N. Barnett, U. Landman, and A. Nitzan, J. Chem. Phys. **89,** 2242 (1988).
[27] R. N. Barnett, U. Landman, and A. Nitzan, Phys. Rev. Lett. **62,** 106 (1989); J. Chem. Phys. **91,** 5567 (1989).
[28] A. Selloni, P. Carenvali, R. Car, and M. Parrinello, Phys. Rev. Lett. **59,** 823 (1987), and Refs. 5–8 therein.
[29] R. B. Gerber, V. Busch, and M. A. Ratner, J. Chem. Phys. **77,** 2022 (1982); R. B. Gerber, R. Kosloff, and M. Berman, Comp. Phys. Report **5,** 59 (1986).
[30] R. Alimi and R. B. Gerber, Phys. Rev. Lett. **64,** 1453 (1990).
[31] W. L. Jorgensen, J. Chandrasekhar, J. D. Madura, R. W. Impey, and M. L. Klein, J. Chem. Phys. **79,** 926 (1983).
[32] J. R. Reimers, R. O. Watts, and M. L. Klein, Chem. Phys. **64,** 95 (1982).
[33] J. R. Reimers and R. O. Watts, Chem. Phys. **85,** 83 (1984); **64,** 95 (1982). Some typographical errors in Refs. 32 and 33 are corrected in Ref. 34.
[34] R. N. Barnett, U. Landman, C. L. Cleveland, and J. Jortner, J. Chem. Phys. **88,** 4421 (1988).
[35] R. N. Barnett, U. Landman, C. L. Cleveland, and J. Jortner, J. Chem. Phys. **88,** 4429 (1988).
[36] J. Schnitker and P. J. Rossky, J. Chem. Phys. **86,** 3462 (1987).
[37] R. N. Barnett, U. Landman, C. L. Cleveland, and J. Jortner, Chem. Phys. Lett. **145,** 382 (1988).
[38] J. Schnitker, K. Motakabbir, P. J. Rossky, and R. Friesner, Phys. Rev. Lett. **60,** 456 (1988).
[39] See references cited in Refs. 34, 35, and 48.
[40] (a) J. V. Coe, G. H. Lee, J. G. Eaton, S. T. Arnold, H. W. Sarkes, K. H Bowen, C. Ludewigt, H. Haberland, and D. R. Worsnop, J. Chem. Phys **92,** 3980 (1990); (b) L. A. Posey and M. A. Johnson (to be published) L. A. Posey, thesis, Yale, 1989.
[41] A. Migus, Y. Gaudel, J. L. Martin, and A. Antonetti, Phys. Rev. Lett. **58** 1559 (1987).
[42] F. H. Long, H. Lu, and K. B. Eisenthal, Phys. Rev. Lett. **64,** 1469 (1990).
[43] R. N. Barnett, U. Landman, and A. Nitzan J. Chem. Phys. (to be published).
[44] J. Anderson, J. J. Ullo, and S. Yip, J. Chem. Phys. **87,** 1726 (1987).
[45] L. A. Posey, J. Chem. Phys. **89,** 4807 (1988); L. A. Posey, P. J. Campagnola, M. A. Johnson, G. H. Lee, J. G. Eaton, and K. H. Bowen (to be published).
[46] A. Bar-on and R. Naaman, J. Chem. Phys. **90,** 5198 (1989).
[47] P. J. Campagnola, L. A. Posey, and M. A. Johnson, J. Chem. Phys. **92,** 3243 (1990).
[48] J. Jortner, U. Landman, and R. N. Barnett, Chem. Phys. Lett. **152,** 352 (1988).
[49] J. D. Jackson, *Classical Electrodynamics*, 2nd ed. (Wiley, New York, 1975).
[50] C. J. F. Bottcher, *The Theory of Electric Polarization*, 2nd ed. (Elsevier, Amsterdam, 1973).
[51] R. A. Marcus, J. Chem. Phys. **24,** 979 (1956).
[52] J. Jortner, Mol. Phys. **5,** 257 (1962).
[53] P. R. Antoniewicz, G. T. Bennett, and J. C. Thomson, J. Chem. Phys. **77,** 4573 (1982).
[54] V. M. Nabutovskii and D. A. Romanov, Sov. J. Low Temp. Phys. **11,** 277 (1985).
[55] M. V. Rama Krishna and K. B. Whaley, Phys. Rev. B **38,** 11839 (1988).
[56] D. Scharf, J. Jortner, and U. Landman, J. Chem. Phys. **88,** 4273 (1988).
[57] J. R. Fox and H. C. J. Anderson, J. Phys. Chem. **88,** 4019 (1984).
[58] The energy distributions for the excited states are slightly biased in the high energy end (this is particularly true for the surface states and for the interior states of the 64 cluster) because the highest energy states obtained for some cluster configurations were too extended to fit on the grid and their energy is therefore biased upwards. This is true also for the spectra shown in Fig. 5, however the effect on the spectra is insignificant because the magnitude of the transition dipole to such states is very small.
[59] The RWK2 potential when applied to water molecules with mass density 1 g/cm^3 using periodic boundary conditions yields a small negative pressure. When restricted to pressure $P=0$ the density is $\rho \sim 1.07$ g/cm^3 (this is the density in the middle of our bigger clusters). Therefore the energies obtained in a $P=0$ simulation will be somewhat different than in a $\rho = 1$ g/cm^3 simulation. For 256 water molecules, periodic boundary conditions and potential cutoff at ~ 18 a.u. the average vertical binding energies are ~ -2.9 eV in the $\rho = 1$ g/cm^3 simulation, and ~ -3.2 eV in the $P=0$ simulation.
[60] We have consistently obtained the left edge of the absorption band of the interior $(H_2O)^-_{64}$ state a little red shifted relative to the $(H_2O)^-_{128}$ and $(H_2O)^-_{256}$ interior state spectra. This may coincide with the dielectric theory result (Fig. 3). However, even if true this effect is marginal relative to the overall line shapes.